Structural Engineering and Mechanics, *Vol. 49, No. 3 (2014) 373-393*
DOI: http://dx.doi.org/10.12989/sem.2014.49.3.373

FE modeling of inelastic behavior of reinforced high-strength concrete continuous beams

Tiejiong Lou[1], Sergio M.R. Lopes[*1] and Adelino V. Lopes[2]

[1]*CEMUC, Department of Civil Engineering, University of Coimbra, Coimbra 3030-788, Portugal*
[2]*Department of Civil Engineering, University of Coimbra, Coimbra 3030-788, Portugal*

(Received November 5, 2012, Revised December 18, 2013, Accepted December 27, 2013)

Abstract. A finite element model for predicting the entire nonlinear behavior of reinforced high-strength concrete continuous beams is described. The model is based on the moment-curvature relations pre-generated through section analysis, and is formulated utilizing the Timoshenko beam theory. The validity of the model is verified with experimental results of a series of continuous high-strength concrete beam specimens. Some important aspects of behavior of the beams having different tensile reinforcement ratios are evaluated. In addition, a parametric study is carried out on continuous high-strength concrete beams with practical dimensions to examine the effect of tensile reinforcement on the degree of moment redistribution. The analysis shows that the tensile reinforcement in continuous high-strength concrete beams affects significantly the member behavior, namely, the flexural cracking stiffness, flexural ductility, neutral axis depth and redistribution of moments. It is also found that the relation between the tensile reinforcement ratios at critical negative and positive moment regions has great influence on the moment redistribution, while the importance of this factor is neglected in various codes.

Keywords: high-strength concrete; beams; moment redistribution; finite element method

1. Introduction

The advance in construction material technology has made it possible to manufacture high-performance concretes, featured by great improvement with regard to mechanical characteristics, workability and durability. Due to its attractive advantages, high-strength concrete has been broadly used in special structures, such as cross-sea bridges, where the strength, durability and serviceability are of particular concern. Also, the utilization of high-strength concrete in normal constructions is expected to be popular.

It is well known that high-strength concrete is more fragile when compared to normal-strength concrete. The fragility of high-strength concrete gave rise to some doubts of its use in structures, since the ductile capacity of the structures is very important from a point of view of structural safety, particularly in high seismic regions. Over last 15 years, many experimental and theoretical studies have been conducted to examine the ductile behavior and plastic rotation of reinforced high-strength concrete beams (Arslan and Cihanli 2010, Bernardo and Lopes 2004, 2009, Carmo

*Corresponding author, Professor, E-mail: sergio@dec.uc.pt

http://www.techno-press.org/?journal=sem&subpage=8 ISSN: 1225-4568 (Print), 1598-6217 (Online)

and Lopes 2005, 2008, Cucchiara *et al*. 2012, Kassoul and Bougara 2010, Ko *et al*. 2001, Kwan *et al*. 2004, Lopes and Bernardo 2003, Lopes and Carmo 2006, Pam *et al*. 2001, Yang *et al*. 2012) and columns (Foster 2001, Foster and Attard 2001, Tan and Nguyen 2005, Campione *et al*. 2006, 2012). The studies generally showed the high-strength concrete members have sufficient ductility to guarantee their structural safety provided that an appropriate choice of the amount and location of the reinforcement is made, and that the general rules adopted for normal-strength concrete structures can also be applied to high-strength concrete structures.

So far, most of the previous works concerning the behavior of high-strength concrete structures focused on statically determinate structures such as simply supported beams. In fact, in practical engineering, the statically indeterminate structures, such as frames and continuous beams, are more common. Due to the existence of redundant restraints, the behavior of continuous beams may introduce different aspects, which implies that the overall behavior of the structures can be quite different from that of simply supported beams. In continuous beams, some redistribution of moments might take place when the constituent materials begin to exhibit inelastic behavior. The redistribution of moments is a very important characteristic of continuous beams and should be well taken into consideration in the ultimate design of such type of beams. However, the moment redistribution behavior as well as other flexural characteristics of continuous high-strength concrete beams is yet to be well understood, since few studies on this topic are available (Carmo and Lopes 2005, 2008).

This article presents a finite element (FE) model developed to predict the complete response of continuous high-strength concrete beams from zero loads up to the ultimate. The FE method is based on the moment-curvature relations and is formulated using the Timoshenko beam theory. The proposed analysis is used to reproduce the experimental results of a series of two-span continuous high-strength concrete beam specimens. A parametric study is carried out on continuous beams with practical dimensions. Emphasis of the numerical evaluation is placed on the effect of tensile reinforcement and the redistribution of moments in continuous reinforced high-strength concrete beams.

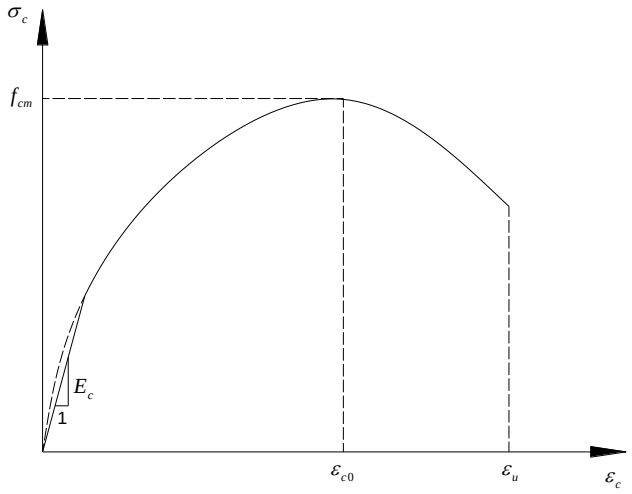

Fig. 1 Stress-strain diagram for unconfined concrete in compression

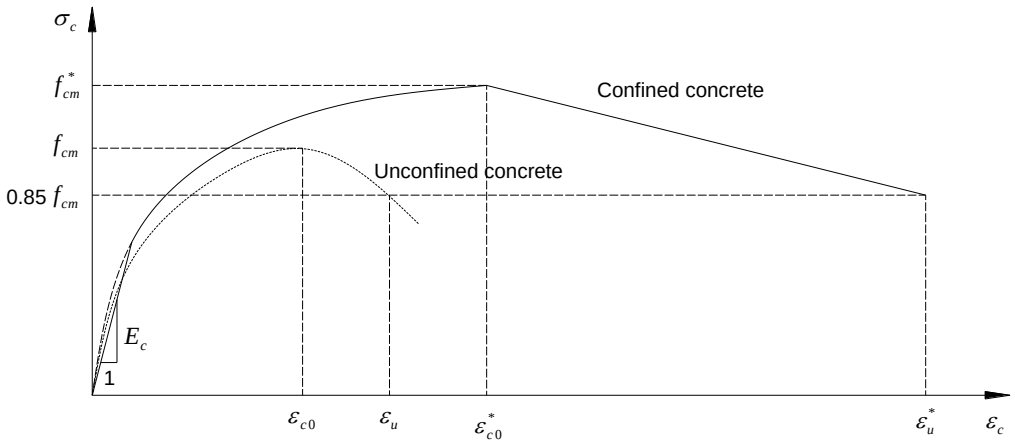

Fig. 2 Stress-strain diagram for confined concrete in compression

2. Material constitutive laws

2.1 Stress-strain law for concrete in compression

In this study, the stress-strain behavior for unconfined concrete is simulated using the model recommended by Eurocode 2 (EC2) (CEN 2004) and Mode Code 1990 (MC90) (CEB-FIP 1990). The stress-strain diagram is shown schematically in Fig. 1, and is expressed as follows

$$\frac{\sigma_c}{f_{cm}} = \frac{k\eta - \eta^2}{1 + (k-2)\eta} \tag{1}$$

where

$$\eta = \varepsilon_c / \varepsilon_{c0} \tag{2}$$

$$k = 1.05 E_c \varepsilon_{c0} / f_{cm} \tag{3}$$

$$f_{cm} = f_{ck} + 8 \tag{4}$$

$$\varepsilon_{c0}(‰) = 0.7 f_{cm}^{0.31} \tag{5}$$

$$E_c = 22(f_{cm}/10)^{0.3} \tag{6}$$

in which σ_c and ε_c are the concrete stress and strain, respectively; f_{cm} is the mean compressive strength (in MPa); f_{ck} is the characteristic cylinder compressive strength (in MPa); ε_{c0} is the concrete strain at peak stress; E_c is the modulus of elasticity of concrete (in GPa). Eq. (1) is valid for $0<|\varepsilon_c|<|\varepsilon_u|$, where ε_u is the ultimate concrete compressive strain determined by

$$\varepsilon_u(‰) = 3.5 \quad \text{for} \quad f_{ck} < 50 \text{ MPa} \tag{7a}$$

$$\varepsilon_u(‰) = 2.8 + 27[(98 - f_{cm})/100]^4 \quad \text{for} \quad f_{ck} \geq 50 \text{ MPa} \tag{7b}$$

To facilitate the numerical modeling, it is assumed that, at initial loading, the concrete in compression is linear elastic until the elastic stress and strain meet the curve equation represented by Eq. (1), as illustrated in Fig. 1.

MC90 also defined a model for confined concrete, which is a modification of the unconfined model by adjusting the magnitude of some key parameters, namely, the concrete strength, the strain at peak stress and the ultimate strain, as shown in Fig. 2. In the absence of more precise data, the relations between the parameters for confined concrete and those for unconfined concrete may be expressed as follows

$$f_{cm}^* = f_{cm}(1.0 + 2.5\alpha\omega_w) \quad \text{for} \quad \sigma_2 \leq 0.05 f_{cm} \tag{8a}$$

$$f_{cm}^* = f_{cm}(1.125 + 1.25\alpha\omega_w) \quad \text{for} \quad \sigma_2 > 0.05 f_{cm} \tag{8b}$$

$$\varepsilon_{c0}^* = \varepsilon_{c0}(f_{cm}^* / f_{cm})^2 \tag{9}$$

$$\varepsilon_u^* = \varepsilon_u + 0.1\alpha\omega_w \tag{10}$$

where f_{cm}^*, ε_{c0}^*, and ε_u^* are the confined strength, confined strain at peak stress and confined ultimate strain, respectively; ω_w is the volumetric mechanical ratio of confining steel; α is the effectiveness of confinement, equal to $\alpha_n\alpha_s$, where α_n depends on the arrangement of stirrups in the cross section and α_s depends on the spacing of stirrups; and σ_2 is the effective lateral compression stress due to confinement.

2.2 Stress-strain law for concrete in tension

The stress-strain behavior for concrete in tension is modeled by a linear-elastic law prior to cracking and by a bilinear tension-stiffening law after cracking, as shown in Fig. 3, where f_t is the tensile strength and ε_{cr} is the cracking strain, equal to f_t/E_c. The tensile strength is determined in terms of the recommendation by EC2:
for concrete class not higher than C50/60

$$f_t = 0.3 f_{ck}^{2/3} \tag{11a}$$

for concrete class higher than C50/60

$$f_t = 2.12 \ln(1 + f_{cm}/10) \tag{11b}$$

2.3 Stress-strain law for reinforcing steel

The stress-strain behavior for reinforcing steel in both tension and compression is modeled by a bilinear elastic-hardening law, as shown in Fig. 4, where σ_s and ε_s are the steel stress and strain, respectively; f_y and f_{su} are the yield strength and ultimate tensile strength of reinforcing steel, respectively; E_s is the modulus of elasticity of reinforcing steel; and ε_{su} is the ultimate steel strain, which is taken as 0.075 in this study.

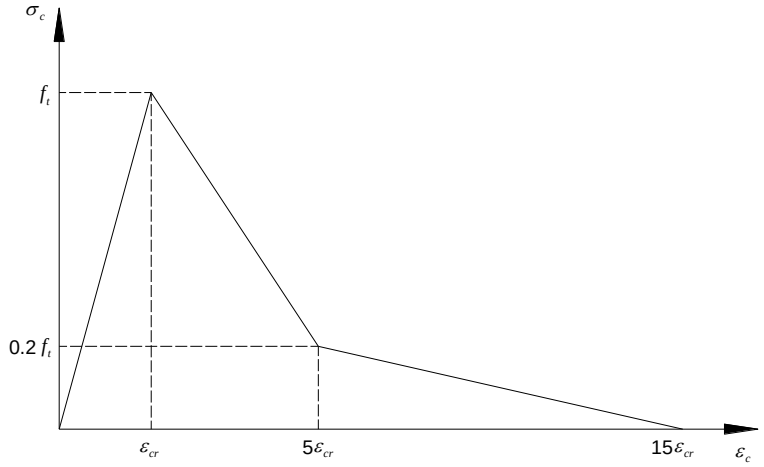

Fig. 3 Stress-strain diagram for concrete in tension

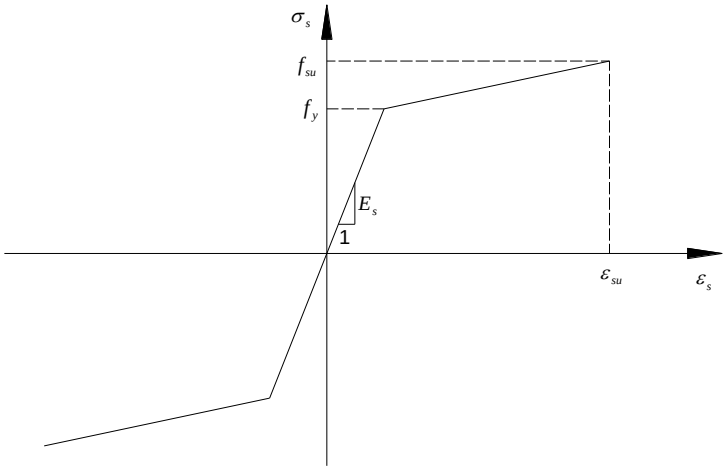

Fig. 4 Stress-strain diagram for reinforcing steel

3. Moment-curvature relations

To establish the moment-curvature relations of reinforced concrete sections, the sections are divided into many concrete layers and reinforcement layers, as shown in Fig. 5. The strain in each concrete layer is assumed to be constant, and equal to the value at the center of the layer. Each reinforcement layer represents the steel bars at the level of the layer. The analysis assumes that a plane section remains plane after deformation, and that the reinforcement perfectly bonds with the surrounding concrete. Based on these assumptions, as shown in Fig. 5, the axial strain at any fiber of the cross sections is given by

$$\varepsilon = \phi y \tag{12}$$

where ϕ is the section curvature, and y is the distance from the neutral axis.

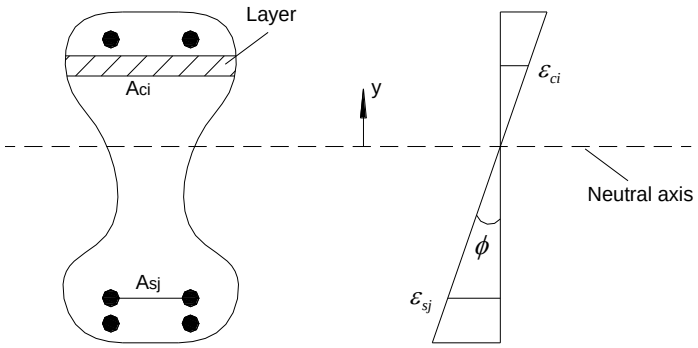

Fig. 5 Section and strain

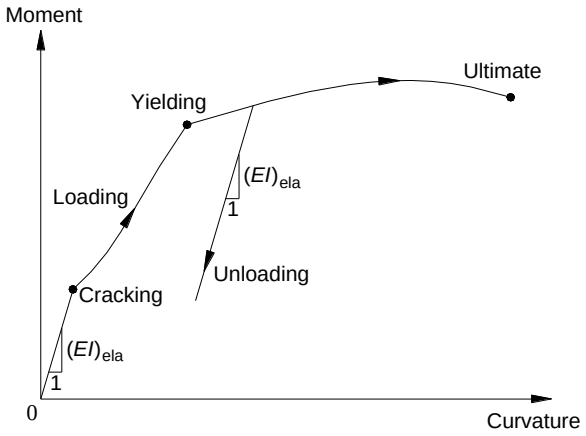

Fig. 6 Moment-curvature diagram for reinforced concrete section

Assuming that the cross sections are subjected to bending moment M (zero axial force), the axial and flexural equilibriums of the sections can be respectively expressed as

$$0 = \sum_i \sigma_{ci} A_{ci} + \sum_j \sigma_{sj} A_{sj} \tag{13}$$

$$M = \sum_i \sigma_{ci} A_{ci} y_{ci} + \sum_j \sigma_{sj} A_{sj} y_{sj} \tag{14}$$

where σ is the stress and A is the area; the subscript ci represents each concrete layer and sj represents each reinforcement layer; the summation is made for all concrete or reinforcement layers.

The moment-curvature relations of beam sections are generated by incrementally varying the prescribed curvature starting from zero value. The ultimate failure of the sections occurs when the compressive concrete or tensile reinforcement reaches its ultimate strain. The procedure for determining the complete moment-curvature relation of a cross section is summarized as follows:

(1) Increase the value of the curvature (initial curvature of zero) with a small step;

(2) Determine the strains in steel and concrete using Eq. (12) based on an assumed initial or the previous neutral axis depth (generally, the initial position of the neutral axis can be taken as the position of the centroidal axis);

(3) Assess the stress in each concrete or reinforcement layer based on the stress-strain laws of the materials;

(4) Calculate the total axial force contributed by the concrete and reinforcement using the right side of Eq. (13);

(5) Check the axial equilibrium of the section; if the equilibrium is not satisfied, adjust the position of the neutral axis until the unbalanced axial force is vanished;

(6) Compute the bending moment using Eq. (14);

(7) Repeat from step (1) until failure of the section.

The typical moment-curvature diagram for a reinforced concrete section is shown schematically in Fig. 6. During the whole loading process, the moment-curvature response would experience three stages. The first stage is characterized by elastic behavior and is finished by concrete cracking. This is followed by the second stage up to steel yielding and then the third stage until the ultimate failure. In the case of unloading, it is assumed that the moment decreases linearly with the curvature, and the slope of decrease is equal to the elastic flexural stiffness $(EI)_{ela}$, as shown in Fig. 6.

4. FE method

The FE method is formulated using the Timoshenko beam theory. In this theory, it is assumed that a plane section normal to the centroidal axis before deformation remains plane but does not remain normal to the centroidal axis after deformation because of the effect of transverse shear deformations. In a two-node element, the transverse displacement w and rotation θ can be expressed as functions of their respective nodal displacements

$$w = N_1 w_1 + N_2 w_2 , \quad \theta = N_1 \theta_1 + N_2 \theta_2 \tag{15}$$

Where $N_1 = (x_2 - x)/l$ and $N_2 = (x - x_1)/l$, in which l is the original length of the beam element; x_1, x_2 are the coordinate values for the element nodes, and $x_2 - x_1 = l$.

The curvature ϕ and shear strain γ can be expressed respectively as follows:

$$\phi = -\frac{\mathrm{d}\theta}{\mathrm{d}x} = -\frac{\mathrm{d}N_1}{\mathrm{d}x}\theta_1 - \frac{\mathrm{d}N_2}{\mathrm{d}x}\theta_2 = \boldsymbol{B}_b \boldsymbol{u}^e \tag{16}$$

$$\gamma = \frac{\mathrm{d}w}{\mathrm{d}x} - \theta = \frac{\mathrm{d}N_1}{\mathrm{d}x} w_1 - N_1\theta_1 + \frac{\mathrm{d}N_2}{\mathrm{d}x} w_2 - N_2\theta_2 = \boldsymbol{B}_s \boldsymbol{u}^e \tag{17}$$

where

$$\boldsymbol{u}^e = \{w_1 \quad \theta_1 \quad w_2 \quad \theta_2\}^{\mathrm{T}} \tag{18}$$

$$\boldsymbol{B}_b = [0 \quad -\frac{\mathrm{d}N_1}{\mathrm{d}x} \quad 0 \quad -\frac{\mathrm{d}N_2}{\mathrm{d}x}] \tag{19}$$

$$\boldsymbol{B}_s = [\frac{\mathrm{d}N_1}{\mathrm{d}x} \quad -N_1 \quad \frac{\mathrm{d}N_2}{\mathrm{d}x} \quad -N_2] \tag{20}$$

The bending moment M and shear force Q can be expressed respectively as follows:

$$M = (EI)\phi = (EI)\boldsymbol{B}_b\boldsymbol{u}^e \tag{21}$$

$$Q = (GA/k)\gamma = (GA/k)\boldsymbol{B}_s\boldsymbol{u}^e \tag{22}$$

where EI is the flexural stiffness, which is obtained from the pre-generated moment-curvature relation; GA is the shear stiffness, which is assumed to be unchanged during the loading process; k is the shear correction factor to allow for cross-sectional warping. In this study, the value of k is taken as 1.2 for a rectangular section.

Based on the virtual work principle, the following element force equilibrium equations can be established

$$\boldsymbol{P}^e = \int_l \boldsymbol{B}_b^{\mathrm{T}} M\mathrm{d}x + \int_l \boldsymbol{B}_s^{\mathrm{T}} Q\mathrm{d}x \tag{23}$$

where $\boldsymbol{P}^e$ is the element equivalent nodal loads

$$\boldsymbol{P}^e = \{Q_1 \quad M_1 \quad Q_2 \quad M_2\}^{\mathrm{T}} \tag{24}$$

Substituting Eqs. (21) and (22) into Eq. (23) yields element stiffness equations

$$\boldsymbol{P}^e = \boldsymbol{K}^e\boldsymbol{u}^e = (\boldsymbol{K}_b^e + \boldsymbol{K}_s^e)\boldsymbol{u}^e \tag{25}$$

where

$$\boldsymbol{K}_b^e = \int_l \boldsymbol{B}_b^{\mathrm{T}}(EI)\boldsymbol{B}_b\mathrm{d}x \tag{26}$$

$$\boldsymbol{K}_s^e = \int_l \boldsymbol{B}_s^{\mathrm{T}}(GA/k)\boldsymbol{B}_s\mathrm{d}x \tag{27}$$

The forms of $\boldsymbol{K}_b^e$ and $\boldsymbol{K}_s^e$ are evaluated using the one-point Gauss quadrature rule.

The stiffness equations for the structure are assembled in the global coordinate system from the contribution of all the beam elements. After applying a proper boundary condition, the nonlinear equilibrium equations are solved by the incremental-iterative method. The iterative scheme for an incremental step is summarized as follows:

(1) Form or update the element stiffness matrices, and assemble them into the structure stiffness matrix;

(2) Solve equilibrium equations for displacement increments, and add them to the previous total to get the current nodal displacements;

(3) In the local coordinate system, compute the element curvature using Eq. (16) and element shear strain using Eq. (17);

(4) Use the moment-curvature relation to determine the bending moment M and to update the flexural stiffness EI, and use Eq. (22) to compute the shear force Q;

(5) Determine the element end forces using the right side of Eq. (23) and then assemble them into the internal resisting loads;

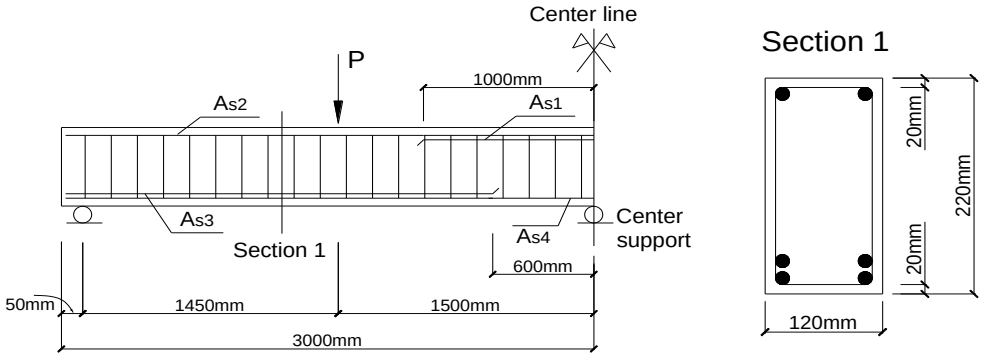

Fig. 7 Details of experimental beams

Table 1 Amount of longitudinal reinforcement in experimental beams

Beam	A_{s1} (mm^2)	A_{s2} (mm^2)	A_{s3} (mm^2)	A_{s4} (mm^2)
V1-0.7	157 (2Ø 10)	157 (2Ø 10)	383 (2Ø 10+2Ø 12)	157 (2Ø 10)
V1-1.4	314 (2Ø 10+2Ø 10)	157 (2Ø 10)	383 (2Ø 10+2Ø 12)	157 (2Ø 10)
V1-2.1	452 (2Ø 12+2Ø 12)	226 (2Ø 12)	559 (2Ø 10+2Ø 16)	157 (2Ø 10)
V1-2.9	628 (2Ø 16+2Ø 12)	402 (2Ø 16)	854 (2Ø 12+2Ø 20)	226 (2Ø 12)
V1-3.8	804 (2Ø 16+2Ø 16)	402 (2Ø 16)	854 (2Ø 12+2Ø 20)	226 (2Ø 12)
V1-5.0	1030 (2Ø 16+2Ø 20)	402 (2Ø 16)	854 (2Ø 12+2Ø 20)	226 (2Ø 12)

(6) Compute the out-of-balance loads for the next iteration.

5. Numerical application

5.1 Experimental beams

In an experimental program conducted in Coimbra (Carmo 2004, Carmo and Lopes 2005, 2008), a group of 6 reinforced high-strength concrete continuous beams, designated as V1-0.7, V1-1.4, V1-2.1, V1-2.9, V1-3.8 and V1-5.0, were tested up to failure. The main variable of the test was the amount of tensile reinforcement at the negative moment region, which varied from 157 (V1-0.7) to 1030 mm^2 (V1-5.0). The specimens were of a rectangular section with width of 120 mm and depth of 220 mm, and were 6000 mm long with two spans symmetric with respect to the center line crossing the center support, as illustrated in Fig. 7.

The layout and amount of reinforcement (A_{s1}, A_{s2}, A_{s3} and A_{s4}) are presented in Fig. 7 and Table 1. The longitudinal reinforcement consisted of 10, 12, 16 or 20 mm deformed steel bars having average yield strength of 569 MPa and tensile strength of 669 MPa. The shear reinforcement consisted of 6 mm stirrups with spacing of 100 mm in the outer shear spans, and of 8 mm stirrups

with spacing of 100 mm in the inner shear spans. The average concrete strength at 28 days for the specimens is 71 MPa. The product $\alpha\omega_w$ in Eqs. (8) and (10) is taken as 0.016 in the analysis to consider the confinement of concrete. More details about the specimens have been reported elsewhere (Carmo 2004, Carmo and Lopes 2005, 2008).

5.2 Analysis and comparison

The proposed model is used to perform the analysis of the experimental beams. Due to symmetry, half of the beam is considered and divided into 19 beam elements (1 element for the part outside the end support, 9 elements with equal length for the part between end support and loading point, and 9 elements with equal length for the part between center support and loading point). The self-weight of the beams is converted into uniform load (0.66 kN/m).

It is observed that over the entire loading process, all the analyzed beams but V1-5.0 experience sequentially five typical phases, namely, the onset of concrete cracking at the center support (first cracking), the onset of concrete cracking at the span critical section located at the loading point (second cracking), the beginning of reinforcement yielding at the center support (first yielding), the beginning of reinforcement yielding at the span critical section (second yielding), and crushing of concrete. For Beam V1-5.0, the first yielding appears at the span critical section, followed by the second yielding at the center support.

Fig. 8 shows the comparison between predicted and experimental results in relation to the load-deflection response of the beams. The finite element analysis (FEA) exhibits an overestimation of the pre-cracking stiffness and cracking loads of the beams. This can be explained that in the pre-cracking stage, the concrete may not display perfectly elastic behavior as assumed in the analysis, and that the concrete tensile strength calculated by Eq. (11b) may be overestimated. However, the overall responses predicted by the analysis agree well with the experimental ones for all beams except for V1-2.1. For Beam V1-2.1, the predicted ultimate load is obviously lower than the experimental value. This may be attributed to that the actual material property of tensile reinforcement in this beam is different from the value adopted in the analysis.

5.3 Moment-curvature response

The numerical results regarding the moment-curvature response at the center support section of the beams are shown in Fig. 9. The entire response is characterized by three stages separated by two points corresponding to concrete cracking and reinforcement yielding, respectively. Because the behavior in the first stage (elastic stage) is mainly controlled by the concrete, the responses in this stage and the cracking moments for the beams are almost the same. After cracking, the contribution of reinforcement becomes increasingly important, so the responses for the beams differ. The higher the amount of reinforcement, the stiffer the beam, as expected.

The flexural curvature ductility, μ_ϕ, of a section can be defined by

$$\mu_\phi = \frac{\phi_u}{\phi_y} \tag{28}$$

in which ϕ_u, ϕ_y are the curvatures at the ultimate limit state and at the beginning of tensile reinforcement yielding, respectively.

A list of values of ϕ_y, ϕ_u and μ_ϕ at the center support section of the beams is given in Table 2. It

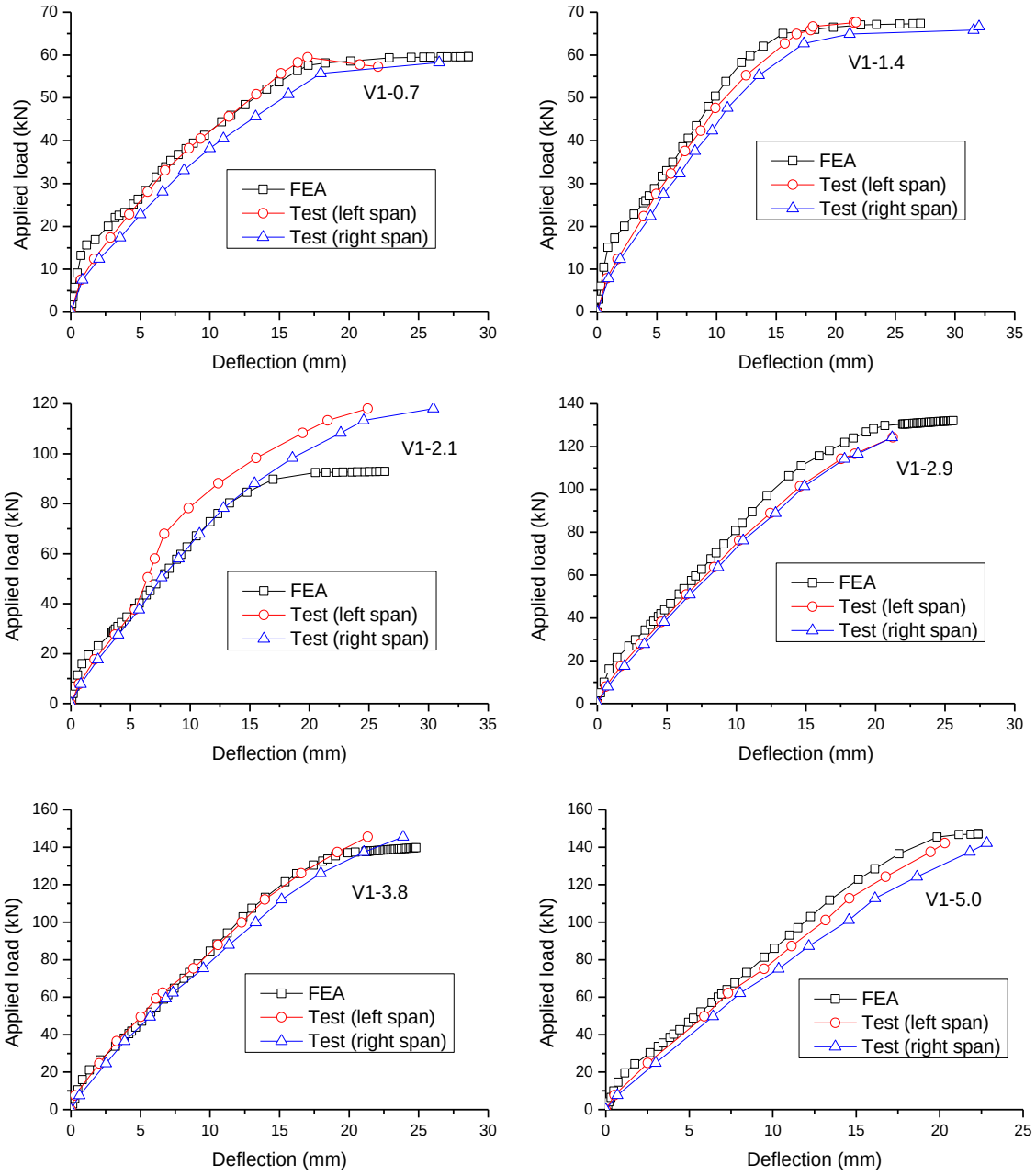

Fig. 8 Comparison between predicted load-deflection response and experimental results for the specimens

is seen that a higher amount of tensile reinforcement mobilizes a higher value of ϕ_y but a lower value of ϕ_u, leading to a much lower curvature ductility.

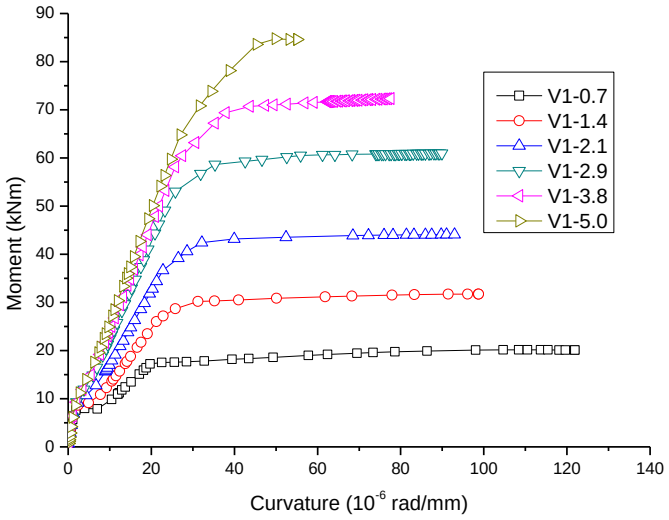

Fig. 9 Moment-curvature response for the specimens according to numerical prediction

Table 2 Values of curvature ductility and curvatures at yielding and ultimate for the specimens according to numerical prediction

Beam	ϕ_y (10^{-6} rad/mm)	ϕ_u (10^{-6} rad/mm)	μ_ϕ
V1-0.7	20.33	121.91	6.00
V1-1.4	21.76	98.73	4.54
V1-2.1	23.01	92.97	4.04
V1-2.9	25.20	89.92	3.57
V1-3.8	26.48	77.58	2.93
V1-5.0	27.91	55.12	1.97

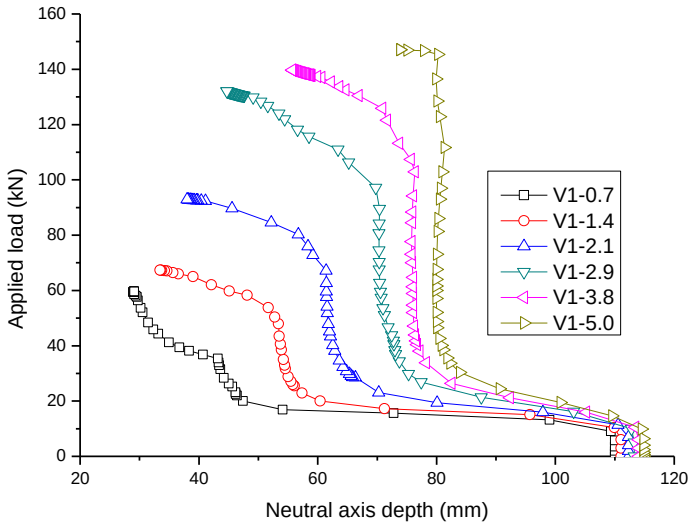

Fig. 10 Variation of neutral axis depth with applied load for the specimens according to numerical prediction

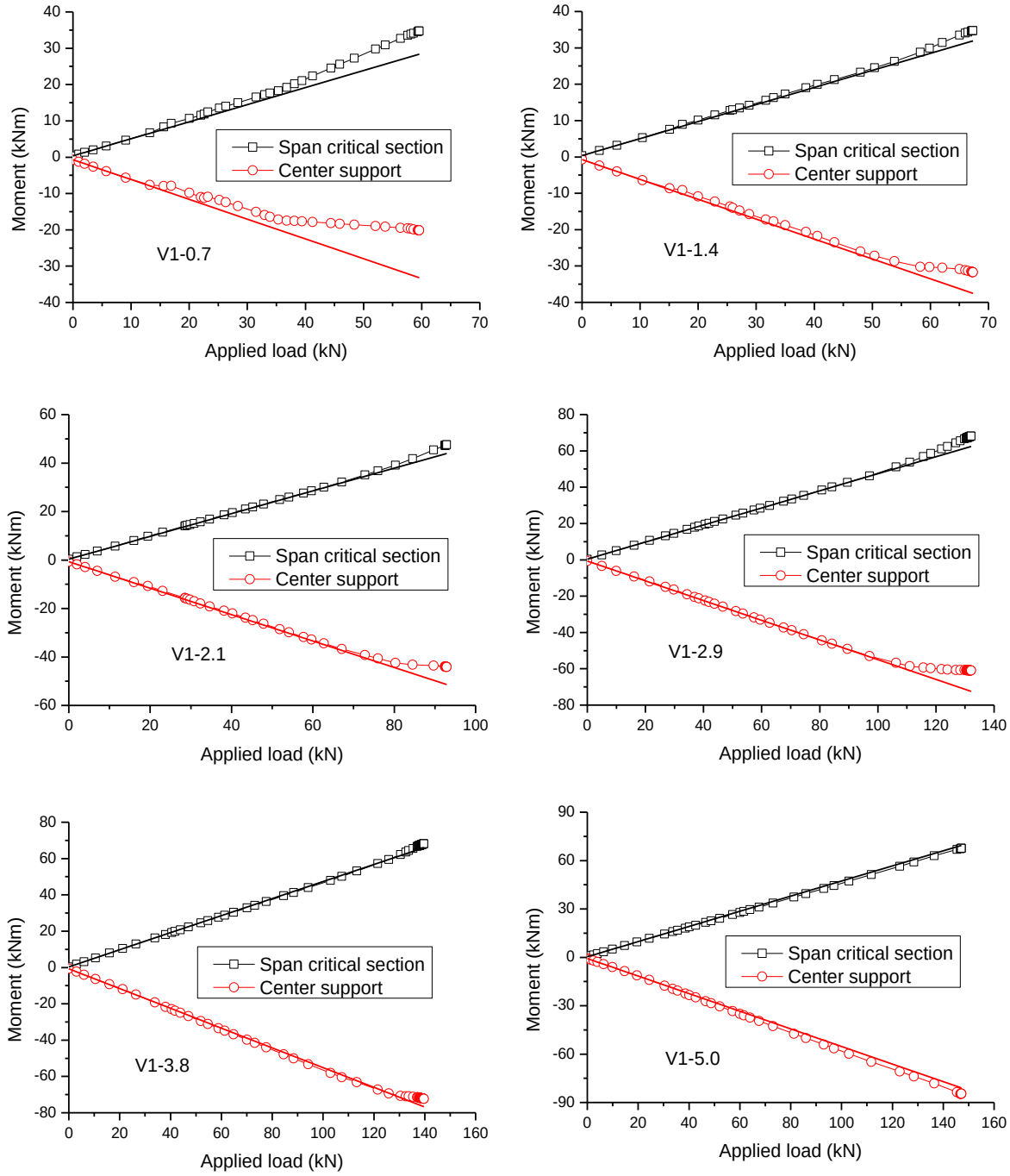

Fig. 11 Moment evolution with applied load for the specimens according to numerical prediction

5.4 Variation of neutral axis depth

Fig. 10 shows the numerical results regarding the variation of the neutral axis depth at the center support section with the applied load. The evolution of the neutral axis depth can be characterized by four stages separated by three points corresponding to concrete cracking, stabilization of crack development, and reinforcement yielding, respectively. In the first stage, the position of neutral axis is at the place of centroidal axis of the transformed section and remains unchanged. This is followed by the second stage, characterized by a significant drop of the neutral axis depth with a small increase in the applied load. The behavior in the third stage is opposite to that in the second stage, that is, the movement of the neutral axis is insignificant while the increase in the applied load is great. After the tensile reinforcement in the center support section yields (in the last stage), a quick drop of the neutral axis depth with the applied load is observed. It is also observed that at the ultimate limit state, a higher amount of tensile reinforcement results in a larger neutral axis depth, as expected.

5.5 Moment redistribution

Fig. 11 shows the numerical results regarding the development of bending moments at the span critical section and center support with the applied load. The straight line in the graph represents the elastic values, which are calculated assuming the constituent materials are linear elastic. Due to redistribution of moments, the moment evolution in a beam might be influenced by cracking of concrete and yielding of reinforcement (formation of plastic hinges), while the extent of influence is dependent on the content of tensile reinforcement. For beams with low amounts of tensile reinforcement (Beams V1-0.7 and V1-1.4), the actual moment, computed by FEA, begins to deviate from the elastic value at the onset of cracking. This is followed by a stabilizing trend until yielding of the tensile reinforcement at the center support, which causes an accentuated trend of deviation between actual and elastic moments due to further redistribution of moments from the center support region to the span critical region. In comparison with Beam V1-1.4, the above observation is more obvious for Beam V1-0.7 due mainly to the larger stiffness difference between critical positive and negative moment regions. On the other hand, for beams with high reinforcement ratios, concrete cracking (for V1-2.1, V1-2.9 and V1-3.8) and/or reinforcement yielding (for V1-5.0) may not have a noticeable effect on the moment redistribution, as shown in Fig. 11.

The degree of moment redistribution, β, can be expressed as

$$\beta = 1 - \frac{M_u}{M_e} \tag{29}$$

where M_u is ultimate actual moment, computed by FEA in this study; and M_e is the elastic moment corresponding to the ultimate load.

A summary of values of the actual and elastic moments and the degree of moment redistribution at the span critical and center support sections of the experimental beams is given in Table 3. It is observed that at the ultimate limit state, all specimens but V1-5.0 have positive (negative) redistribution at the center support (span critical section). Beam V1-5.0, in which the tensile reinforcement ratio at the negative moment region is higher than that at the positive moment region, on the other hand, shows a negative (positive) redistribution at the center support

Table 3 Values of actual, elastic moments and the degree of moment redistribution for the specimens according to numerical prediction

Beam	M_u (kN·m)		M_e (kN·m)		β (%)	
	Span critical	Center support	Span critical	Center support	Span critical	Center support
V1-0.7	34.76	-20.12	28.35	-33.17	-22.63	39.34
V1-1.4	34.76	-31.71	31.91	-37.52	-8.94	15.47
V1-2.1	47.53	-44.10	43.96	-51.36	-8.12	14.15
V1-2.9	68.12	-60.97	62.48	-72.45	-9.03	15.85
V1-3.8	68.15	-72.31	65.99	-76.71	-3.28	5.74
V1-5.0	67.61	-84.58	69.42	-80.89	2.61	-4.56

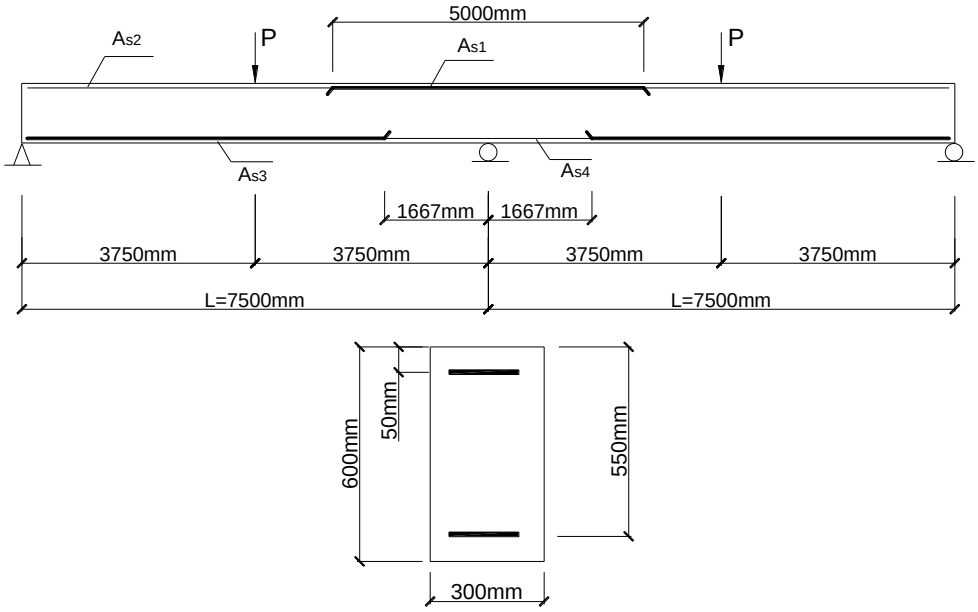

Fig. 12 Details of the reference beam used for parametric evaluation

(span critical section). This observation can be attributed to the fact that the moments are prone to redistributed from the weaker sections to the stronger sections. In addition, it is generally observed that the degree of moment redistribution decreases with the increase of the tensile reinforcement ratio. However, a higher tensile reinforcement ratio (V1-2.9) may exhibits higher redistribution than do lower reinforcement ratios (V1-2.1 and V1-1.4). This can be explained that the stiffness difference between critical positive and negative moment regions in V1-2.9 is larger than those in V1-1.4 and V1-2.1 The larger the stiffness difference, the higher the redistribution of moments.

6. Effect of tensile reinforcement on the value of β

In this section, a parametric study is carried out to examine the effect of tensile reinforcement on the value of β. A two-span continuous beam with practical dimensions as shown in Fig. 12 is

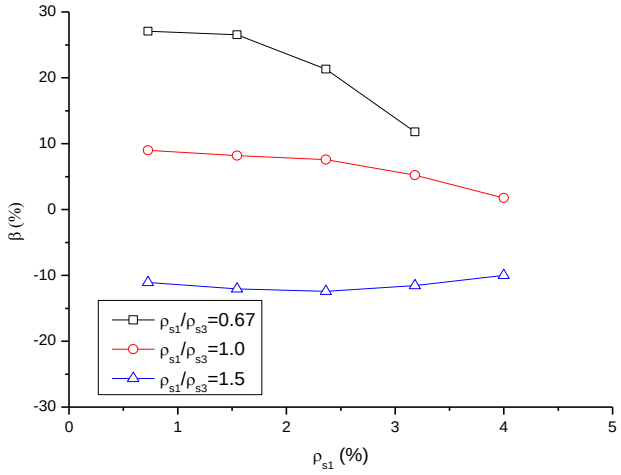

Fig. 13 Effect of ρ_{s1} and ρ_{s1}/ρ_{s3} on the degree of moment redistribution according to numerical prediction

used to illustrate the results obtained from the analysis. Two important factors related to the tensile reinforcement are evaluated, namely, the tensile reinforcement ratio at the center support ρ_{s1} or at midspan ρ_{s3}, and the ratio ρ_{s1}/ρ_{s3}. Three levels of ρ_{s1}/ρ_{s3} are considered, namely, 0.67, 1.0 and 1.5; the factor ρ_{s1} varies from 0.73% to 4% for ρ_{s1}/ρ_{s3} of 1.0 and 1.5, and to 3.18% for ρ_{s1}/ρ_{s3} of 0.67. The compressive reinforcement ratios at the center support ρ_{s4} and at midspan ρ_{s2} are taken as 0.36%. The concrete is assumed to be unconfined. The material properties are assumed to be the same as those of the experimental beams described above, that is, the concrete strength is taken as 71 MPa, and the steel yield strength is taken as 569 MPa.

Fig. 13 illustrates the influence of ρ_{s1} and ρ_{s1}/ρ_{s3} on the degree of moment redistribution at the center support section. It is seen that the factor ρ_{s1} affects the degree of moment redistribution differently, depending on the level of the ratio ρ_{s1}/ρ_{s3}. For ρ_{s1}/ρ_{s3} of 0.67 (that is, the tensile reinforcement ratio at the center support is obviously lower than that at midspan), the degree of moment redistribution decrease slightly as ρ_{s1} increases up to 1.55%; with continuing increase of ρ_{s1}, however, the degree of moment redistribution decreases quickly. For ρ_{s1}/ρ_{s3} of 1.0 (that is, the tensile reinforcement ratio at the center support is comparable to that at midspan), the degree of moment redistribution decreases slowly as ρ_{s1} increases. For ρ_{s1}/ρ_{s3} of 1.5 (that is, the tensile reinforcement ratio at the center support is obviously higher than that at midspan), on the other hand, the variation of the degree of moment redistribution with varying ρ_{s1} is not so obvious.

Also, it can be observed from Fig. 13 that the ratio ρ_{s1}/ρ_{s3} has great influence on the redistribution of moments. At a given level of ρ_{s1}, a higher value of ρ_{s1}/ρ_{s3} leas to a much lower value of β at the center support section. The difference between the values of β for different ρ_{s1}/ρ_{s3} levels is particularly significant at low levels of ρ_{s1}. There can be positive or negative redistribution of moments at the center support, depending on the level of ρ_{s1}/ρ_{s3}. When ρ_{s1}/ρ_{s3} is not greater than 1.0, the moment redistribution at the center support is positive. On the other hand, when ρ_{s1}/ρ_{s3} is greater than 1.0, there may appear negative redistribution of moments at the center support.

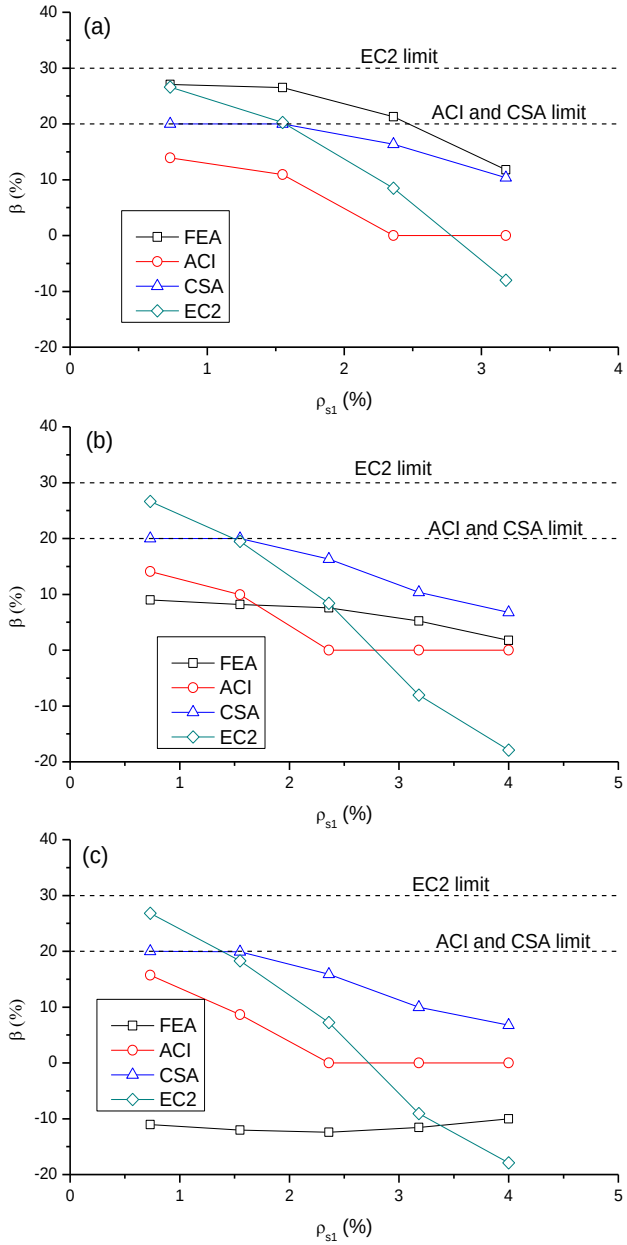

Fig. 14 Variation of β with ρ_{s1} in terms of FEA and various codes. (a) ρ_{s1}/ρ_{s3} =0.67; (b) ρ_{s1}/ρ_{s3} =1.0; (c) ρ_{s1}/ρ_{s3} =1.5.

To take advantage of the ductility of continuous concrete members, the codes allow designers to use a linear elastic analysis with allowable redistribution of moments through the use of the coefficient β.

In the ACI code (ACI Committee 318 2011), the modification of factored moments calculated by elastic theory shall not be more than 1000 ε_t percent, to a maximum of 20%, where ε_t is the net

Table 4 Predictions of moment redistribution by FEA and various codes

ρ_{s1}/ρ_{s3}	ρ_{s1} (%)	M_u (kN·m)	M_e (kN·m)	ε_t (%)	c/d (%)	β (%)			
						FEA	ACI	CSA	EC2
0.67	0.73	-432.11	-592.40	1.39	14.10	27.06	13.90	20.00	26.61
	1.55	-860.27	-1170.72	1.09	18.73	26.52	10.91	20.00	20.25
	2.36	-1271.24	-1615.23	0.73	27.29	21.30	0.00	16.35	8.47
	3.18	-1642.37	-1861.45	0.43	39.29	11.77	0.00	10.36	-8.02
1.0	0.73	-422.05	-463.73	1.41	14.08	8.99	14.09	20.00	26.64
	1.55	-836.92	-911.45	0.99	19.28	8.18	9.92	20.00	19.50
	2.36	-1247.55	-1349.72	0.73	27.34	7.57	0.00	16.33	8.40
	3.18	-1626.76	-1716.24	0.43	39.31	5.21	0.00	10.35	-8.05
	4.00	-1930.04	-1964.24	0.32	46.48	1.74	0.00	6.76	-17.91
1.5	0.73	-417.34	-375.76	1.57	13.95	-11.06	15.72	20.00	26.82
	1.55	-819.27	-731.16	0.87	20.17	-12.05	8.67	19.92	18.27
	2.36	-1221.08	-1085.97	0.66	28.18	-12.44	0.00	15.91	7.25
	3.18	-1593.53	-1428.47	0.40	40.05	-11.56	0.00	9.97	-9.07
	4.00	-1909.01	-1735.50	0.32	46.48	-10.00	0.00	6.76	-17.91

strain in extreme tension steel. The moment redistribution can be made only when ε_t is not less than 0.0075 at the section where the moment is reduced.

In the CSA code (Canadian Standards Association 2004), the negative moment calculated by an elastic analysis can be increased or decreased by not greater than (30−50c/d) percent, with a maximum of 20%, where c/d is the ratio of the neutral axis depth to the effective depth of a cross section.

In EC2 (CEN 2004), the moments at the ultimate limit state computed by a linear elastic analysis can be redistributed by not higher than [0.56−1.25(0.6+0.0014/ε_u)c/d] for concrete strength equal to or below 50 MPa, and by [0.46−1.25(0.6+0.0014/ε_u)c/d] for concrete strength greater than 50 MPa. The maximum redistribution is 30% for high- and normal-ductility steel and of 20% for low-ductility steel.

A comparison of the degrees of moment redistribution at the center support calculated by various codes with the FEA values is summarized in Table 4 and Fig. 14. It is seen in the table and Fig. 14(a) that for ρ_{s1}/ρ_{s3} equal to 0.67, all the codes can well reflect the actual trend of the variation of β with varying ρ_{s1}, although the CSA code shows a smaller slope while EC2 exhibits an obviously sharper slope. All codes are conservative. However, the ACI code seems to be over-conservative over the entire range of ρ_{s1}, while EC2 may be over-conservative at high levels of ρ_{s1}.

On the other hand, for ρ_{s1}/ρ_{s3} equal to 1.0, the variation trends of β predicted by various codes, particularly by EC2, are more significant than that by FEA, as shown in Fig. 14(b). In addition, the CSA code is non-conservative over the entire range of ρ_{s1}, while the ACI code and EC2 may be non-conservative at low levels of ρ_{s1}. From Fig. 14(c), it can be observed that for ρ_{s1}/ρ_{s3} equal to 1.5, all the codes fail to reflect the actual trend of the variation of β. Also, all codes are non-conservative, except EC2 at a very high level of ρ_{s1}.

Fig. 15 illustrates the effect of ρ_{s1}/ρ_{s3} on the value of β according to predictions by various codes. Because either the parameter ε_t or c/d, which is used to calculate the degree of moment

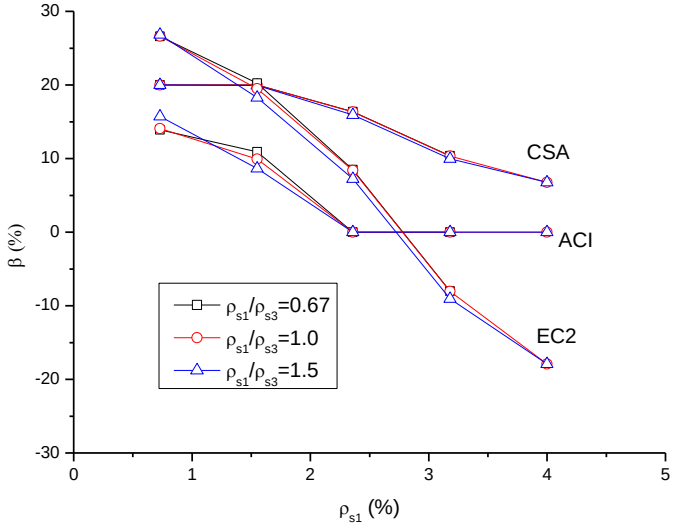

Fig. 15 Effect of ρ_{s1}/ρ_{s3} on the value of β according to code predictions

redistribution in design codes, is almost independent of ρ_{s1}/ρ_{s3}, the great importance of the ratio ρ_{s1}/ρ_{s3} as mentioned previously is neglected in all the codes. Probably, a different parameter that would be somehow related with ρ_{s1}/ρ_{s3} could be more effective for practical design purposes. Therefore, the authors recommend that an extensive study should be carried out in order to find the best parameter to be included in the new simplified rules in codes.

7. Conclusions

A FE model based on the moment-curvature relations is developed to predict the nonlinear behavior of reinforced high-strength concrete continuous beams throughout the loading process. The moment-curvature relations of reinforced concrete sections are pre-generated through section analysis by satisfying the force equilibrium and strain compatibility. The FE method is formulated using the Timoshenko beam theory so as to take into account the effect of shear deformations.

A group of six continuous high-strength concrete beam specimens, where the main variable was the amount of tensile reinforcement, is selected to calibrate the proposed model and to illustrate the results of a numerical evaluation. The results produced by the analysis indicate that the tensile reinforcement has significant influence on the behavior of continuous reinforced high-strength concrete beams, namely, the flexural stiffness, ductility, neutral axis depth and redistribution of moments. It is found that a higher tensile reinforcement ratio results in a greater flexural stiffness after cracking and a higher neutral axis depth at ultimate, but leads to lower ductile behavior and less redistribution of moments.

A parametric study is conducted on two-span high-strength concrete continuous beams with practical dimensions to evaluate the influence of tensile reinforcement on the degree of moment redistribution. Two important factors related to tensile reinforcement, ρ_{s1} and ρ_{s1}/ρ_{s3}, are examined. The study shows that the effect of ρ_{s1} on the degree of moment redistribution is quite different for different levels of ρ_{s1}/ρ_{s3}. The ratio ρ_{s1}/ρ_{s3} is found to be a very important parameter influencing the

redistribution of moments. However, the great importance of this factor is not reflected in various codes.

Acknowledgments

This research is sponsored by FEDER funds through the program COMPETE - Programa Operacional Factores de Competitividade - and by national funds through FCT - Fundação para a Ciência e a Tecnologia -, under the project PEst-C/EME/UI0285/2013. The work presented in this paper has also been supported by FCT under Grant No. SFRH/BPD/66453/2009.

References

ACI Committee 318 (2011), "Building code requirements for structural concrete (ACI 318-11) and commentary", American Concrete Institute, Farmington Hills, MI.

Arslan, G. and Cihanli, E. (2010), "Curvature ductility prediction of reinforced high-strength concrete beam sections", *J. Civil Eng. Manage.*, **16**(4), 462-470.

Bernardo, L.F.A. and Lopes, S.M.R. (2004), "Neutral axis depth versus flexural ductility in high-strength concrete beams", *ASCE J. Struct. Eng.*, **130**(3), 452-459.

Bernardo, L.F.A. and Lopes, S.M.R. (2009), "Plastic analysis of HSC beams in flexure", *Mater. Struct.*, **42**, 51-69.

Campione, G., Fossetti, M., Minafò, G. and Papia, M. (2012), "Influence of steel reinforcements on the behavior of compressed high strength R.C. circular columns", *Eng. Struct.*, **34**, 371-382.

Campione, G., Fossetti, M. and Papia, M. (2006), "Simplified analytical model for compressed high-strength columns confined by transverse steel and longitudinal bars", *Proceedings of 2nd International FIB Congress*, Naples, Italy.

Canadian Standards Association (2004), "Design of concrete structures (A23.3-04)", Mississauga, Ontario, Canada.

Carmo, R.N.F. (2004), "Plastic rotation and moment redistribution in high strength concrete beams", PhD Thesis, University of Coimbra, Coimbra, Portugal. (in Portuguese)

Carmo, R.N.F. and Lopes, S.M.R. (2005), "Ductility and linear analysis with moment redistribution in reinforced high-strength concrete beams", *Can. J. Civil Eng.*, **32**, 194-203.

Carmo, R.N.F. and Lopes, S.M.R. (2008), "Available plastic rotation in continuous high-strength concrete beams", *Can. J. Civil Eng.*, **35**, 1152-1162.

CEB-FIP (1990), "Model code for concrete structures", Euro-International Committee for Concrete - International Federation for Prestressing, Thomas Telford Services Ltd., Lausanne, Switzerland.

CEN (2004), "Eurocode 2: Design of concrete structures - Part 1-1: General rules and rules for buildings", EN 1992-1-1, European Committee for Standardization, Brussels, Belgium.

Cucchiara, C., Fossetti, M. and Papia, M. (2012), "Steel fibre and transverse reinforcement effects on the behaviour of high strength concrete beams", *Struct. Eng. Mech.*, **42**(4), 551-570.

Foster, S.J. (2001), "On behavior of high-strength concrete columns: cover spalling, steel fibers, and ductility", *ACI Struct. J.*, **98**(4), 583-589.

Foster, S.J. and Attard, M.M. (2001), "Strength and ductility of fiber-reinforced high-strength concrete columns", *ASCE J. Struct. Eng.*, **127**(1), 28-34.

Kassoul, A. and Bougara, A. (2010), "Maximum ratio of longitudinal tensile reinforcement in high strength doubly reinforced concrete beams designed according to Eurocode 8", *Eng. Struct.*, **32**, 3206-3213.

Ko, M.Y., Kim, S.W. and Kim, J.K. (2001), "Experimental study on the plastic rotation capacity of reinforced high strength concrete beams", *Mater. Struct.*, **34**, 302-311.

Kwan, A.K.H., Au, F.T.K. and Chau, S.L. (2004), "Theoretical study on effect of confinement on flexural ductility of normal and high-strength concrete beams", *Mag. Concrete Res.*, **56**(5), 299-309.

Lopes, S.M.R. and Bernardo, L.F.A. (2003), "Plastic rotation capacity of high-strength concrete beams", *Mater. Struct.*, **36** 22-31.

Lopes, S.M.R. and Carmo, R.N.F. (2006), "Deformable strut and tie model for the calculation of the plastic rotation capacity", *Comput. Struct.*, **84**, 2174-2183.

Pam, H.J., Kwan, A.K.H. and Ho, J.C.M. (2001), "Post-peak behavior and flexural ductility of doubly reinforced normal- and high-strength concrete beams", *Struct. Eng. Mech.*, **12**(5), 459-474.

Tan, T.H. and Nguyen, N.B. (2005), "Flexural behavior of confined high-strength concrete columns", *ACI Struct. J.*, **102**(2), 198-205.

Yang, J.M., Min, K.H. and Yoon, Y.S. (2012), "Effect of anchorage and strength of stirrups on shear behavior of high-strength concrete beams", *Struct. Eng. Mech.*, **41**(3), 407-420.